Water Air Soil Pollut (2022) 233: 65
https://doi.org/10.1007/s11270-022-05528-6

Potential Application of Alternative Materials for Organic Pollutant Removal

Matheus Londero da Costa · Giovani Pavoski · Denise Crocce Romano Espinosa · Noeli Júlia Schüssler de Vasconcellos · William Leonardo da Silva

Received: 2 November 2021 / Accepted: 26 January 2022 / Published online: 12 February 2022

Abstract The work aims to synthesize and characterize vegetal charcoal (or biochar) from Syzygium cumini (AC-SC), evaluating the adsorption capacity for dexamethasone drug (DEX) removal, using the kinetic and equilibrium adsorption. The samples were characterized by N_2 porosimetry, X-ray diffraction, scanning electron microscopy with energy-dispersive spectroscopy, zeta potential, and zero charge point. Adsorption equilibrium was carried out applying the Langmuir, Freundlich, Redlich-Peterson, Sips, and Toth models, and kinetic adsorption applied the pseudo-first order, pseudo-second order, Elovich, Avrami, and Weber-Morris models. AC-SC showed a heterogeneous and porous surface, negatively charged, crystalline structure, specific surface area of the 2.14 $m^2\ g^{-1}$ and $pH_{ZCP} = 7.36$. About the effect of the AC-SC concentration, 5.0 g L^{-1} showed the best DEX removal (53.02%), about the others' concentration (2.0 and 7.5 g L^{-1}). About the equilibrium and kinetic adsorption, the Sips model and pseudo-second order showed the best experimental data adjusted, indicating that the adsorption monolayer was dependent on the ions onto the biosorbent, with a maximum adsorption capacity of 0.744 mg g^{-1} after 180 min. Therefore, AC-SC can be used as an alternative material in the removal of organic pollutants, such as drug removal.

Keywords *Syzygium cumini* · Biosorption · Biochar · Adsorption · Dexamethasone

1 Introduction

Water is an essential resource for the permanence of life on the Earth; however, due to the significant increase of pollution on hydro resources, it is necessary to act on preserving these resources to avoid social and environmental crises (Empinotti et al., 2019).

Concurrently, COVID-19 caused by the SARS-CoV-2 showed a serious problem about the drug consummation, mainly the dexamethasone, being a corticosteroid medication used for the treatment of chronic obstructive pulmonary diseases, reducing the inflammatory process associated with the exacerbated production of cytokines, as well as pulmonary edema and alveolar damage (Halpin et al., 2020; Sterne, 2020). However, around 65% of the

M. L. da Costa · W. L. da Silva (✉)
Chemical Engineering Course, Franciscan University, Santa Maria, Brazil
e-mail: w.silva@ufn.edu.br

G. Pavoski · D. C. R. Espinosa
Polytechnical School of Chemical Engineering, University of São Paulo, São Paulo, SP, Brazil

N. J. S. de Vasconcellos
Environmental and Sanitary Engineering Course, Franciscan University, Santa Maria, Brazil

W. L. da Silva
Nanoscience Graduate Program, Franciscan University, Santa Maria, Brazil

dexamethasone, after being absorbed in the gastrointestinal tract, is excreted by the urine, being able to generate by-products after 24 h (Nunes & Lima, 2020; Wang et al., 2020). Thus, advanced processes for the treatment of drug wastewater have been studied to provide the correct and adequate treatments for these effluents (Oliveira et al., 2020) such as adsorption.

Adsorption is the physical or chemical adhesion of atoms, ions, or molecules of the organic pollutants onto the surface of a solid (labeled adsorbent) (Wang et al., 2019). Moreover, this process has as main characteristics a low complexity, low operating cost, and the possibility of the use of alternative materials (biosorbents) to remove drugs, such as cellulose sources (Zhu et al., 2018), chitosan (Yanyan et al., 2018), and residual biomass (Gallo-Cordova et al., 2017).

Biochar or vegetal charcoal has been used in the adsorption process because of its application variability of alternative materials, which can be synthesized with many (agro)industrial residues from high-carbon precursors, showing high porosity and specific surface area and stability (Srivatsav et al., 2020), being favorable in removing drugs (Kebede et al., 2020), such as tetracycline (Smiljanić et al., 2021), ibuprofen, and naproxen (Ahsan et al., 2018). Moreover, vegetal charcoal can be synthesized from different methods, highlighting the activation/carbonization process from various residual biomass using the step of thermal degradation and the activation with activating agent (Chi et al., 2021). Among the main novelties and advantages for the use of biochar are the following (Albanio et al., 2021; Costa et al., 2021): (a) economic: due to operational simplicity and the possibility of using different residual biomasses with high availability; (b) environmental: contributes to the mitigation of climate change and the reuse of residual biomass, preventing these residues from becoming possible environmental liabilities; and (c) high adsorption capacity to remove organic pollutants with easy adsorbate recovery and biosorbent reusability.

In this context, the present work aims to synthesize and characterize biochar (or vegetal charcoal) from *Syzygium cumini* leaves, to evaluate the adsorption capacity for dexamethasone drug (DEX) using kinetic and equilibrium study.

2 Materials and Methods

2.1 Preparation of *Syzygium cumini* Leaves

Syzygium cumini leaves were obtained from a local property (Santa Maria – RS, Brazil), where they were successively washed with potable water (about 5 times), drying (60 °C for 24 h), and ground in a knife mill for 15 min, being sieved for uniform particle size (#12).

2.2 Biochar Synthesis

The preparation of the biochar was carried out by the methodology adapted (Zhang, Zhao, et al., 2019), using *Syzygium cumini* leaves. Thus, initially, the leaves were placed under magnetic agitation with zinc chloride ($ZnCl_2$, CAQ, PA) with 1:2 w/w (leaves:$ZnCl_2$) for 30 min. After, the solution was placed on the furnace (heating rate of 30 °C min^{-1}) at 600 °C for 2 h. Figure 1 shows a schematic representation of the biochar preparation process. The sample was labeled as AC-SC.

2.3 Characterization

For the biochar crystallinity characterization, the X-ray diffraction (XRD) was applied using Bruker Optics equipment (D2 Advance, USA) with a copper tube (radiation $K_{\alpha\text{-}Cu} = 1.5418$ Å) and angle range 2θ of the 10° in 70°, acceleration tension and current applied of 30 kV and 30 mA. The N_2 porosimetry was used to determine the specific surface area, diameter,

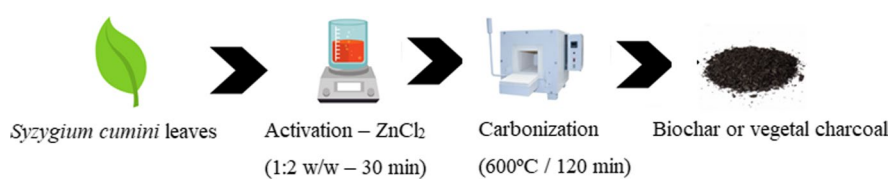

Fig. 1 Schematic representation of the AC-SC preparation process

and volume pore, using the adsorption/desorption isotherms in the Gemini VII 2375 Surface Area Analyzer Micrometrics equipment. For the computation of the specific area (S_{BET}), Brunauer–Emmett–Teller equation (BET method) was used, in the relative pressure ($P\ Po^{-1} = 0.05$ to 0.35), and for the diameter and volume pore diameter the Barret-Joyner-Halenda equation (BJH method). The surface charge was determined using zeta potential (ZP) using Malvern-Zetasizer® version nanoZS (ZEN3600, UK) with closed capillary cells (DTS 1060) (Malvern Instruments, UK) with laser He–Ne of 4 mW (633 nm). To investigate the morphologic properties of the AC-JL, scanning electron microscopy with energy-dispersive spectroscopy (SEM–EDS) was used in the Phenom Prox Scanning Electron Microscope (Thermo Fisher Scientific) using metalized with gold sputtering and submitted to a magnification of the 710× under 15 kV of the voltage. The zero charge point (pH_{ZCP}) was determined according to the 11-point methodology, according to the literature (Bakatula et al., 2018). Thus, 0.1 g of AC-SC was added in solution with DEX at different pH (2, 3, 4, 5, 6, 7, 8, 9, 10, 11, and 12), where this initial pH was adjusted with HCl (Sigma-Aldrich, PA) and NaOH (Sigma-Aldrich, PA), both at 1.0 mol L^{-1}. The final pH was measured after 3 h at 120 rpm of rotation and room temperature (25 ± 2 °C).

2.4 Effect of the AC-SC Concentration and the Adsorption Tests

The adsorption tests were carried out in batch processing over 3 h, where aliquots were collected at predetermined times (0, 5, 15, 30, 45, 60, 75, 90, 120, 150, and 180 min) and evaluated the effect of the concentration of the biochar (2, 5, and 7.5 g L^{-1}). All samples were analyzed at the specific wavelength of the DEX drug ($\lambda_{max} = 242$ nm) (Sastry et al., 2016) and all of the adsorption tests were performed in duplicate (with error values less than 5%).

2.5 Equilibrium Adsorption

Adsorption equilibrium study correlates the number of available active sites present onto the biosorbent surface with the number of drug molecules. Thus, there are a series of models (denominated isotherms) that correlate the adsorption capacity with the equilibrium DEX concentration, mainly Langmuir (Langmuir, 1918), Freundlich (Freundlich, 1906), Sips (Sips, 1948), and Toth (Tóth, 1981), according to Eqs. (1)–(4), respectively.

$$q_e = \frac{q_m * C_e}{1 + k_L * C_e} \tag{1}$$

$$q_e = k_F * C_e^{\frac{1}{n}} \tag{2}$$

$$q_e = \frac{q_s * (k_S * C_e)^{n_S}}{1 + (k_S * C_e)^{n_S}} \tag{3}$$

$$q_e = \frac{q_{To} * C_e}{\left(b_{To} + C_e^{n_{To}}\right)^{n_{To}}} \tag{4}$$

where q_e (mg g^{-1}) and C_e (mg L^{-1}) are adsorbed amount and adsorbate concentrations at equilibrium; q_m, q_S, and q_{To} (mg g^{-1}) are the maximum adsorbed amount to Langmuir, Sips, and Toth, respectively, where the maximum adsorbed amount is influenced according to the concentration of biochar (Bardestani et al., 2019; Zhang, Meng, et al., 2019); K_L is Langmuir constant (L mg^{-1}); k_F is the Freundlich constant ((mg g^{-1}) (mg L^{-1})$^{-1/n}$) which indicates the relative adsorption/desorption capacity of the adsorbent in relation to the bonding energy; n is the constant related to the adsorption intensity that should be between 1 and 10, where it usually indicates physical adsorption (Dasgupta et al., 2018; Enaime et al., 2017); n_s is the heterogeneity factor, where if $n_s = 1$, the model is reduced to the Langmuir equation and if $n_s < 1$, there is an increase in heterogeneity, that is, the model approaches Freundlich (Kumar et al., 2019; Shahri et al., 2018); n_{TO} is the heterogeneity parameter, which can assume a value between 0 and 1; for $n_{TO} = 1$ the Langmuir model is obtained (characteristic for representing homogeneous surfaces) and if $n_{TO} \neq 1$ represents a heterogeneous surface; and b_{TO} is the constant of the Toth isotherm (Al-Ghouti & D.A. Da'ana, 2020; Kumar et al., 2021).

The degree of development and spontaneity of the reaction of adsorption can be obtained from the evaluation of the parameter of equilibrium or separation factor (R_L), which indicates whether the adsorption reaction is favorable or unfavorable (Akrawi et al., 2021), according to Eq. (5).

$$R_L = \frac{1}{1 + k_L * C_e} \tag{5}$$

where the adsorption will be considered favorable if $0 < R_L < 1$, unfavorable to $R_L > 1$, linear ($R_L = 1$), and irreversible ($R_L = 0$).

2.6 Kinetic Adsorption

The kinetic models describe the speed on which the reaction occurs, needing this way the respective times (t), being more usual pseudo-first order (PFO) (Lagergren, 1898), pseudo-second order (PSO) (Blanchard et al., 1984), Elovich (ELO) (Aharoni & Tompkins, 1970), Avrami (AVR) (Avrami, 1939), and Weber-Morris (WEM) (Weber & Morris, 1963), according to Eqs. (6)–(10), respectively.

$$q_t = q_1 * (1 - \mathrm{Exp}(-k_1 * t)) \tag{6}$$

$$q_t = k_2 * \left(q_2^2\right) * \frac{t}{(1 + k_2 * q_2 * t)} \tag{7}$$

$$q_t = \left(\frac{1}{b_e}\right) * \mathrm{ln}(1 + a_e * b_e * t) \tag{8}$$

$$q_t = q_{avr} * (1 - E\mathrm{xp}(-k_{avr} * t)^{n_{avr}} \tag{9}$$

$$q_t = k_{wm} * t^{0.5} + B \tag{10}$$

where k_1 (min^{-1}) is the rate constant of pseudo-first order; q_1, q_2, and q_{avr} (mg g^{-1}) are theoretical values of adsorption capacity; k_2 (g mg^{-1} min^{-1}) is the rate constant of pseudo-second order; b_e (mg g^{-1} min^{-1}) is the initial adsorption rate; a_e (g mg^{-1}) is the desorption constant of the Elovich model; k_{avr} (min^{-1}) is the rate constant of Avrami model; n_{avr} is a heterogeneity factor; and k_{wm} (mg g^{-1} $\mathrm{min}^{-0.5}$) is the intraparticle diffusion rate.

2.7 Statistical Evaluation of Adjusted Models

The kinetic and equilibrium parameters were determined by adjusting the models with the experimental data, using non-linear regression, by Statistic 9.1 software (StatSoft, USA) with the Quasi Newton method. The determination coefficient (R^2), adjusted determination coefficient (R^2_{adj}), root mean square error (RMSE), and error sum of squares (SSE) were used to evaluate the fit quality of the models, according to Eqs. (11)–(14) (Ceylan, 2020; Doiron, 2019; Roozbeh et al., 2020).

$$\mathrm{R}^2 = 1 - \frac{\sum_{\mathrm{i}=1}^{\mathrm{n}} \left(\mathrm{y}_{\mathrm{exp}} - \mathrm{y}_{\mathrm{pred}}\right)^2}{\sum_{\mathrm{i}=1}^{\mathrm{n}} \left(\mathrm{y}_{\mathrm{exp}} - \bar{\mathrm{y}}_{\mathrm{exp}}\right)^2} \tag{11}$$

$$R^2_{adj} = 1 - \left(1 - R^2\right).\left(\frac{n-1}{n-p}\right) \tag{12}$$

$$\mathrm{RMSE} = \sqrt{\sum_{i=1}^{n} \frac{(y_{pred} - y_{exp})^2}{n}} \tag{13}$$

$$\mathrm{SSE} = \frac{1}{\mathrm{n}} \sum_{\mathrm{i}=1}^{\mathrm{n}} \left(\mathrm{y}_{\mathrm{exp}} - \mathrm{y}_{\mathrm{pred}}\right)^2 \tag{14}$$

where $\mathrm{y}_{\mathrm{exp}}$ is the experimental data, $\mathrm{y}_{\mathrm{pred}}$ is the predicted value, n is the number of experimental values, and p is the number of parameters according to the model.

3 Results and Discussion

3.1 Characterization of the Biochar

Figure 2 represents the diffractogram pattern of the AC-SC, showing a crystalline structure of the biochar prepared using an active agent ($ZnCl_2$). Thus, wurtzite-type hexagonal crystalline structures of the ZnO with characteristic peaks and planes were indicated at 31.3° (1 0 0), 33.8° (0 0 2), 35.8° (1 0 1), 46.9° (1 0 2), 56.3° (1 1 0), 62.5° (1 0 3), 66.2° (2 0 0), 67.3° (1 1 2), and 68.5° (2 0 1), according to the Joint Committee on Powder Diffraction Standard (JCPDS—nº 01–075-0576), coming from the precursor of the chemical activation $ZnCl_2$ (Figueiredo et al., 2020; Zidi et al., 2019).

Figure 3a shows the micrograph of AC-SC, indicating a heterogeneous and rough surface, with a series of cavities and porosity, with a measured average diameter of about 53.5 nm. Figure 3b represents the elementary composition (% weight) by EDS, indicating the presence of zinc (65.94%), oxygen

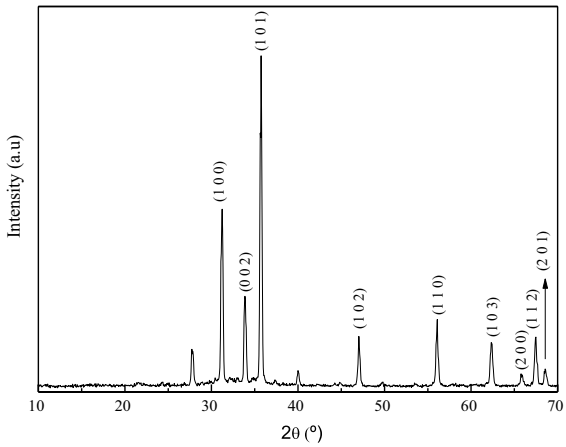

Fig. 2 XRD pattern diffractogram of the AC-SC

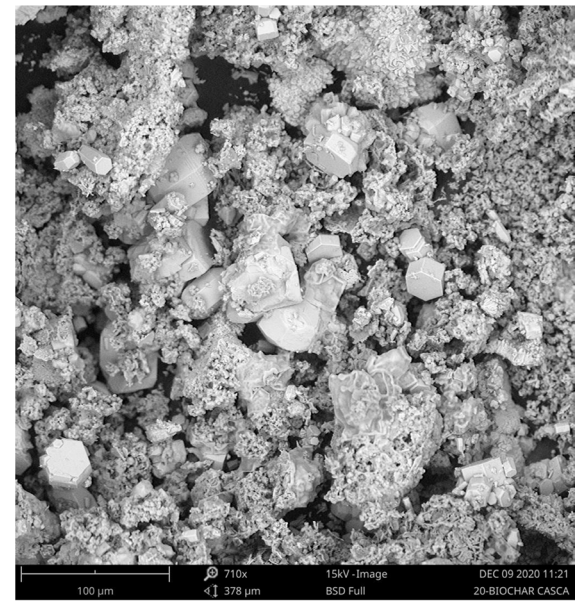

(a)

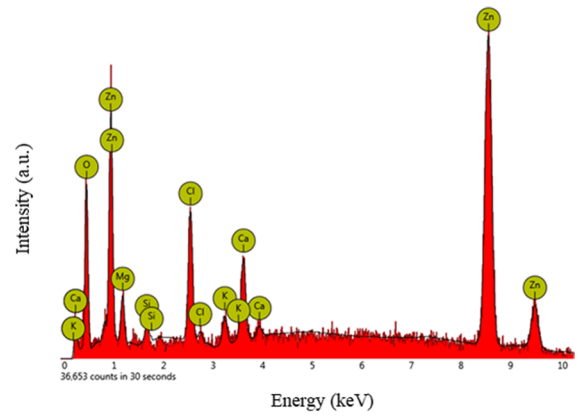

(b)

Fig. 3 **a** SEM micrograph at 710× magnification and **b** elementary composition (% weight) obtained by EDS analysis for the AC-SC.

(21.09%), magnesium (4.37%), chlorine (4.12%), calcium (2.74%), silica (0.88%), and potassium (0.86%).

According to Fig. 3a, it was possible to identify the formation of the zinc oxide (ZnO) crystal onto the biochar surface in the wurtzite-type hexagonal crystalline structure with a lattice parameter of the a = 0.325 nm and c = 0.521 nm, and special group P63mc, indicating that the oxygen atoms are stacked in a compact hexagonal shape and the zinc atoms occupy half of the tetrahedral interstices (Bayan & Mohanta, 2010). Figure 3b indicates the majority presence of zinc and oxygen, confirming the effectiveness of the activation/carbonization process. The other elements found (such as magnesium, chlorine, calcium, silica, and potassium) come from the residual biomass used as a precursor for the preparation of biochar.

Figure 4 represents the N_2 adsorption/desorption isotherms used to determine the specific surface area (S_{BET}), pore diameter (Dp), and pore volume (Vp).

According to Fig. 4, AC-SC showed a structure with hysteresis type H3, indicating plate-like particle aggregates that give rise to wedge-shaped and cone-shaped pores. Moreover, the specific surface area was 2.14 ± 0.10 m^2 g^{-1}, diameter pore (Dp) of the 53.63 ± 0.04 nm and volume pore (Vp) of the 0.0054 ± 0.003 cm^3 g^{-1}, indicating the mesoporous materials, but with smaller specific area and pore volume about other vegetal charcoals, due to the precursor chosen for synthesis and the possible sintering of the pores, decreasing in the surface area and porosity (Liu et al., 2020). However, it allows the possibility of a high removal capacity due to the selectivity of the AC-SC with the dexamethasone drug, allowing a physicochemical interaction and thus the possible removal of the organic pollutant (Pavlović et al., 2021). About the zeta potential (ZP) (pH = 5.5 ± 0.5), AC-SC showed negative surface charge (− 3.09 ± 0.21 mV), due to the composition of precursors (*Syzygium cumini* leaves), such as flavonoids and hydrolyzable tannins, as a group of polyphenols (phenolic rings), indicating the stability of the biosorbent

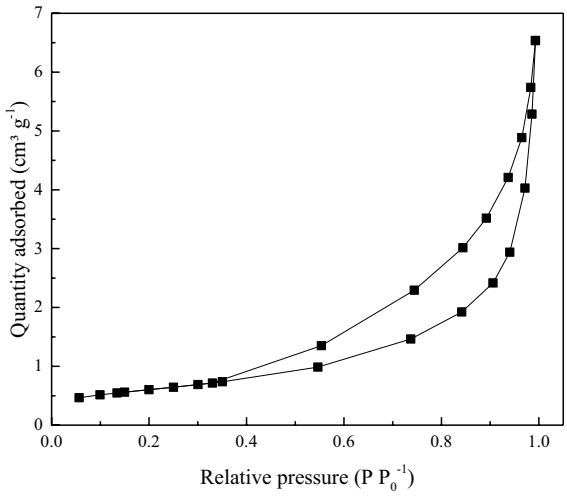

Fig. 4 N_2 adsorption/desorption isotherms of the AC-SC

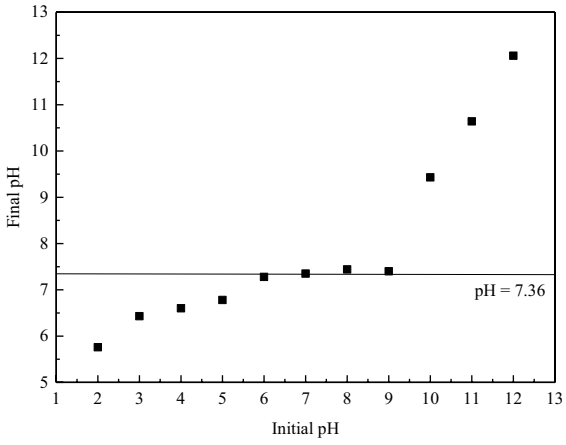

Fig. 5 Zero charge point (pH_{ZCP}) of the AC-SC

and favoring the interaction between the drug and the surface of the AC-SC (Bernardo et al., 2021; Daniel & Devi, 2019; Sethy et al., 2020).

Figure 5 shows the zero charge point (pH_{ZCP}) of the AC-SC, indicating around 7.36, confirmed with the literature (Ghenaatgar et al., 2019). Moreover, when the pH is lower than pH_{ZCP}, AC-SC surface will be protonated, favoring the adsorption of compounds with negative charges (such as drugs), and many anions will be adsorbed to balance the positive charges. Thus, the adsorption process can be explained by the electrostatic attraction between the charge generated on the surface of the adsorbent material and the anionic group of the solution (Thiebault, 2020).

3.2 Equilibrium Adsorption Isotherms

Table 1 presents the results of adsorption equilibrium parameters using biochar in the concentrations of the 2, 5, and 7.5 g L^{-1} and [DEX] = 4 mg L^{-1}, while Table 2 presents the statistical parameters obtained by the adjustment of the experimental data for the equilibrium models. The drug concentration was optimized in a preliminary study and according to the literature (Asuha et al., 2019); thus, [DEX] = 4 mg L^{-1} was chosen for the adsorption tests.

According to Table 1, about the Langmuir model, all the results showed the R_L values between 0 and 1, indicating the adsorption process was considered favorable. Moreover, the maximum adsorption capacity (Q_{max}) increased with the AC-SC concentration, due to the greater number of active sites available for adsorption of the drug and, thus, the greater the rate of diffusion and mass transfer (Bagheri et al., 2020). For Freundlich isotherm, only the concentration of 5 g L^{-1} showed the heterogeneity of the material ($1 < n < 10$). Sips isotherm showed the K_s in the

Table 1 Parameter equilibrium obtained using Langmuir, Freundlich, Sips, and Toth models

[AC-SC] (g L^{-1})	Langmuir			Freundlich			Sips		Toth		
	Q_{max} (mg g^{-1})	K_L (L mg^{-1})	R_L	K_F ((mg g^{-1})(mg $L^{-1})^{-1/n}$)	n	Q_s (mg g^{-1})	K_s (L mg^{-1})	n_s	Q_{to} (mg g^{-1})	B_{to} (L mg^{-1})	n_{to}
2	0.141	0.027	0.479	0.154	1.94	0.272	0.135	−8.205	0.021	1.961	0.193
5	0.673	1.234	0.168	0.383	3.351	0.519	0.393	−5.749	3031	19.87	2.902
7.5	0.744	0.041	0.849	1.9×10^{-4}	0.191	0.769	4.985	−5.337	3008	9250	0.731

Table 2 Statistical parameters regarding the readjustment of experimental results

[AC-SC] (g L^{-1})	Langmuir				Freundlich				Sips				Toth			
	R^2	R^2_{adj}	RMSE	SSE	R^2	R^2_{adj}	RMSE	SSE	R^2	R^2_{adj}	RMSE	SSE	R^2	R^2_{adj}	RMSE	SSE
2	0.270	0.210	0.147	0.068	0. 601	0.568	0.328	0.152	0.847	0.782	0.463	0.214	0.454	0.221	0.876	0.767
5	0.070	0.040	0.038	0.018	0.143	0.091	0.078	0.036	0.984	0.978	0.017	0.001	0.978	0.969	0.021	0.001
7.5	0.046	0.022	0.025	0.012	0.337	0.271	0.184	0.085	0.896	0.851	0.011	0.001	0.567	0.401	0.039	0.001

concentrations of 2 and 5 g L^{-1} had values close to 0; thus, the equation can be reduced to the Freundlich isotherm, and n_s values were below 0, indicating an increase in heterogeneity. About the Toth isotherm, n_{TO} in the concentration of 5 g L^{-1} showed greater heterogeneity due to being greater than 1, and the maximum adsorption capacity Q_{TO} obtained an increase with the increase in the concentration of biochar, where in the 7.5 g L^{-1} there was a saturation due to more than biochar.

About the equilibrium model, the Sips model showed the best fit, according to the coefficient determination (R^2) of 0.847, 0.984, and 0.896 to the 2, 5, and 7.5 g L^{-1} respectively, with a maximum adsorption capacity (Qs) of 0.272, 0.519, and 0.769 mg g^{-1}. Thus, according to the literature, the results using biochar in the removal of drugs were promising, with excellent results for Q_s, K_s, and n_S using the Sips model that, in high concentrations of adsorbate, provides an adsorption capacity in monolayers, characteristic of the isotherm of Langmuir (Nguyen et al., 2021; Santos et al., 2020).

3.3 Kinetic Adsorption Models

For the kinetic study of the adsorption, the pseudo-first order, pseudo-second order, Avrami, and Weber-Morris models were used to obtain the kinetic parameters, according to Table 3. Moreover, Table 4 presents the statistical parameters obtained by the adjustment of the experimental data for the kinetic models. Thus, the pseudo-second order kinetic model showed the best experimental fit of the data for the biochar concentration of 5 ($R^2 = 0.87$) and 7.5 ($R^2 = 0.73$) g L^{-1}, indicating the adsorption mechanism that involves electron exchange and/or transfer between the biochar and the drug, suggesting chemical adsorption (Bullen et al., 2021; Chen et al., 2018; Ezzati, 2020; Hubbe et al., 2019).

In other studies, *Syzygium cumini* leaves were also used to remove organic pollutants, where some equilibrium and kinetic models were used, as shown in Table 5.

Table 5 shows the results of other research using *Syzygium cumini* leaves in the removal of pollutants; the q_{max} was better than that presented in the present study; that is, due to the difference in activation of the biosorbent, there is an increase in the chemical interaction; both obtained a *n* optimal value for

Table 3 Kinetic parameters obtained using the pseudo-first order, pseudo-second order, Elovich, Avrami, and Weber-Morris models

AC-SC (g L^{-1})	Pseudo-first order		Pseudo-second order		Elovich		Avrami			Weber-Morris	
	q_1 (mg g^{-1})	k_1 (1 min^{-1})	q_2 (mg g^{-1})	k_2 (g (mg $min^{-1})^{-1}$	a_e (mg (mg $min^{-1})^-$	b_e (mg g^{-1})	q_{avr} (mg g^{-1})	k_{avr} (L min^{-1})	n_{avr}	k_{wm} (mg (g $min^{0.5})^{-1}$	B (mg g^{-1})
2	1.850	0.123	1.704	1396	1.065	3.001	1.850	0.012	9.772	0.139	0.523
5	0.451	0.257	0.455	1.910	9.95×10^{-6}	558.4	2601	1.7×10^{-4}	0.008	0.015	0.282
7.5	0.093	0.362	0.101	2.952	0.896	90.23	228.0	1.9×10^{-7}	20.01	0.006	0.039

Table 4 Statistical parameters regarding the readjustment of experimental results

AC-SC (g L^{-1})	PFO				PSO				Elovich				Avrami				Weber-Morris			
	R^2	R^2_{adj}	RMSE	SSE	R^2	R^2_{adj}	RMSE	SSE	R^2	R^2_{adj}	RMSE	SSE	R^2	R^2_{adj}	RMSE	SSE	R^2	R^2_{adj}	RMSE	SSE
2	0.26	0.07	1.02	1.05	0.17	0.04	1.09	1.17	0.25	0.06	1.03	1.05	0.25	0.06	1.02	1.05	0.22	0.03	1.05	1.09
5	0.85	0.81	0.05	0.003	0.87	0.75	0.06	0.004	0.80	0.76	0.41	0.18	0.25	0.40	0.27	0.07	0.19	0.08	0.13	0.02
7.5	0.64	0.54	0.02	0.001	0.73	0.62	0.02	0.001	0.69	0.67	0.02	0.001	0.99	0.59	0.05	0.002	0.52	0.39	0.02	0.001

Table 5 Kinetic and equilibrium parameters in the removal of pollutants using *Syzygium cumini* leaves

AC-SC (g L^{-1})	Langmuir			Freundlich		Reference
	Q_{max} (mg g^{-1})	K_L (L mg^{-1})	R_L	K_F ((mg g^{-1})(mg $L^{-1})^{-1/n}$)	n	
25	11.52	0.275	0.879	2.31	1.453	Keshtkar et al., 2019)
6.5	1.121	-	-	-	1.093	Tirkey et al., 2018)
	Pseudo-first order		Pseudo-second order			
	q_1 (mg g^{-1})	k_1 (1 min^{-1})	q_2 (mg g^{-1})	k_2 (g (mg $min^{-1})^{-1}$		
25	0.547	0.021	2.34	0.126		Keshtkar et al., 2019)
6.5	0.0009	0.073	0.4991	2.38		Tirkey et al., 2018)

Freundlich, the pseudo-second order (PSO) kinetic model was the best at the concentration of 6.5 g L^{-1}; this shows the similarity with the result obtained in the present work.

4 Conclusion

It was possible to verify the DEX removal capacity using the AC-SC, presenting a better fit in the Sips equilibrium model with the best R^2 of 0.962, that in high concentrations of adsorbate, provides an adsorption capacity in monolayers, characteristic of the isotherm of Langmuir, and a maximum Q_S adsorption capacity of 0.769 mg g^{-1}, n_S values were below zero, indicating a heterogeneous surface, as also showed by EDS and for the kinetic, the best model obtained was the PSO where the R^2 has a value of 0.87 indicating that the adsorption mechanism that involves electron exchange and/or transfer between the biochar and the drug, suggesting chemical adsorption, in the end of the tests showed removal of 53.02% of DEX drug. The AC-SC showed a heterogeneous surface and a percentage of presence of zinc (65.94%), according to the SEM–EDS, a negatively charged ZP and a zero charge point (pH_{ZCP}) of 7.36. Therefore, biochar presented good results in the removal of DEX, considering the AC-SC can be used as an alternative material in the removal of organic pollutants.

Acknowledgements The authors would like to thank the National Council for Scientific and Technological Development (CNPq), Polytechnical School of Chemical Engineering at University of São Paulo (USP, Brazil – SP), and the Franciscan University for their support to develop this work.

Author Contribution M.L. da Costa: conceptualization, validation, writing—review and editing.

G. Pavoski: conceptualization, data curation, formal analysis, investigation and validation.

D.C.R. Espinosa: conceptualization, data curation, formal analysis, investigation and validation.

N.J.S. De Vasconcellos: conceptualization, validation, writing—review and editing.

W.L. da Silva: conceptualization, data curation, formal analysis, investigation, validation, writing—original draft, writing—review and editing.

Funding This study was financially supported by the Foundation for Research of the State of Rio Grande do Sul (FAPERGS – Project 19/2551–0001362-0).

Availability of Data and Materials The data that support the findings of this study are available on request from the corresponding author.

Declarations

Ethics Approval Not applicable in this work.

Consent to Participate Not applicable.

Consent to Publish All authors read and approved the final manuscript.

Competing Interests The authors declare no competing interests.

References

Aharoni, C., & Tompkins, F. C. (1970). Kinetics of adsorption and desorption and the Elovich equation. *Advances in Catalysis, 21*, 1–49. https://doi.org/10.1016/S0360-0564(08)60563-5

Ahsan, M. A., Jabbari, V., Islam, M. T., Kim, H., Hernandez-Viezcas, J. A., Lin, Y., Díaz-Moreno, C. A., Lopez, J., Gardea-Torresdey, J., & Noveron, J. C. (2018). Green synthesis of a highly efficient biosorbent for organic, pharmaceutical, and heavy metal pollutants removal: Engineering surface chemistry of polymeric biomass of spent coffee waste. *J. Water Process Eng., 25*, 309–319. https://doi.org/10.1016/j.jwpe.2018.08.005

Akrawi, H. S. Y., Al-Obaidi, M. A., & Abdulrahman, C. H. (2021). Evaluation of Langmuir and Frendlich isotherm equation for Zinc Adsorption in some calcareous soil of Erbil province north of Iraq. *IOP Conference Series: Earth and Environmental, 761*, 012017–012028. https://doi.org/10.1088/1755-1315/761/1/012017

Albanio, I. I., Muraro, P. C. L., & Da Silva, W. L. (2021). Rhodamine B dye adsorption onto biochar from olive biomass waste. *Water, Air, and Soil Pollution, 232*, 214–224. https://doi.org/10.1007/s11270-021-05110-6

Al-Ghouti, M. A., & Da'ana, D. A. (2020). Guidelines for the use and interpretation of adsorption isotherm models: A review. *Journal of Hazardous Materials, 393*, 122383–122405. https://doi.org/10.1016/j.jhazmat.2020.122383

Asuha, S., Fei, F., Wurendaodi, W., Zhao, S., Wu, H., & Zhuang, X. (2019). Activation of kaolinite by a low-temperature chemical method and its effect on methylene blue adsorption. *Powder Technology, 361*, 624–632. https://doi.org/10.1016/j.powtec.2019.11.068

M. Avrami, Kinetics of phase change I. General theory, J. Chem. Phys. 7 (1939) 1103–1112. https://doi.org/10.1063/1.1750380.

Bagheri, A., Abu-Danso, E., Iqbal, J., & Bhatnagar, A. (2020). Modified biochar from Moringa seed powder for the removal of diclofenac from aqueous solution. *Environmental Science and Pollution Research, 27*, 7318–7327. https://doi.org/10.1007/s11356-019-06844-x

Bakatula, E. N., Richard, D., Neculita, C. M., & Zagury, G. J. (2018). Determination of point of zero charge of natural organic materials. *Environmental Science and Pollution Research, 25,* 7823–7833. https://doi.org/10.1007/s11356-017-1115-7.

Bardestani, R., Roy, C., & Kaliaguine, S. (2019). The effect of biochar mild air oxidation on the optimization of lead(II) adsorption from wastewater. *Journal of Environmental Management, 240*, 404–420. https://doi.org/10.1016/j.jenvman.2019.03.110

Bayan, S., & Mohanta, D. (2010). Directed growth characteristics and optoelectronic properties of Eu-doped ZnO nanorods and urchins. *Journal of Applied Physics, 108*, 023512–023512. https://doi.org/10.1063/1.3462396

Bernardo, W. L. C., Boriollo, M. F. G., Tonon, C. C., Da Silva, J. J., Cruz, F. M., Martins, A. L., Höfling, J. F., & Spolidorio, D. M. P. (2021). Antimicrobial effects of silver nanoparticles and extracts of *Syzygium cumini* flowers and seeds: Periodontal, cariogenic and opportunistic pathogens. *Archives of Oral Biology, 125*, 105101–105113. https://doi.org/10.1016/j.archoralbio.2021.10

Blanchard, G., Maunaye, M., & Martin, G. (1984). Removal of heavy metals from waters by means of natural zeolites. *Water Research, 18*, 1501–1507. https://doi.org/10.1016/0043-1354(84)90124-6

Bullen, J. C., Saleesongsom, S., Gallagher, K., & Weiss, D. J. (2021). A revised pseudo-second-order kinetic model for adsorption, sensitive to changes in adsorbate and adsorbent concentrations. *Langmuir, 37*, 3189–3201. https://doi.org/10.1021/acs.langmuir.1c00142

Ceylan, Z. (2020). Assessment of agricultural energy consumption of Turkey by MLR and Bayesian optimized SVR and GPR models. *Journal of Forecasting, 39*, 944–956. https://doi.org/10.1002/for.2673

Chen, J., Wang, X., Huang, Y., Lv, S., Cao, X., Yun, J., Cao, D. (2018). Adsorption removal of pollutant dyes in wastewater by nitrogen-doped porous carbons derived from natural leaves. Engineered Science, 5, 30–38. https://doi.org/10.30919/es8d666

Chi, N. T. L., Anto, S., Ahamed, T. S., Kurmar, S. S., Shanmugam, S., Samuel, M. S., Manthimani, T., Brindhadevi, K., & Pugazhendhi, A. (2021). A review on biochar production techniques and biochar based catalyst for biofuel production from algae. *Fuel, 287*, 119411–1194200. https://doi.org/10.1016/j.fuel.2020.119411

M.L. Costa, J.P.M. Resmini, N.J.S. Vasconcellos, W.L. Da Silva, Agroindustrial waste application for drugs biosorption, Disciplinarum Scientia. Série Ciências Naturais e Tecnológicas 22 (2021) 1–16. https://doi.org/10.37779/nt.v22i3.4075.

Daniel, J. A., & Devi, S. A. (2019). Inhibition of key digestive enzymes involved in glucose metabolism by biosynthesized zinc oxide nanoparticles from Syzygium cumini (L.): an in vitro and in silico approach. *Pharmacognosy Magazine, 15*, 502–509. https://doi.org/10.4103/pm.pm_253_19

Dasgupta, A., Matos, J., Muramatsu, H., Ono, Y., Gonzalez, V., Liu, H., Rotella, C., Fujisawa, K., Cruz-Silva, R., Hashimoto, Y., Endo, M., Kaneko, K., Radovic, L. R., &

Terrones, M. (2018). Nanostructured carbon materials for enhanced nitrobenzene adsorption: Physical vs. chemical surface properties. *Carbon, 139*, 833–844. https://doi.org/10.1016/j.carbon.2018.07.045

De Oliveira, M., Frihling, B. E. F., Velasques, J., Filho, F. J. C. M., Cavalheri, P. S., & Migliolo, L. (2020). Pharmaceuticals residues and xenobiotics contaminants: Occurrence, analytical techniques and sustainable alternatives for wastewater treatment. *Science of the Total Environment, 705*, 135568–135640. https://doi.org/10.1016/j.scitotenv.2019.1355

B. Doiron, Electron harvesting and dynamics at a metal-semiconductor interface, Imper. Coll. Lond. Dep. Phys. 1 (2019) 1–231. https://doi.org/10.25560/76495.

Dos Santos, G. E. S., Ide, A. H., Duarte, J. L. S., Mckay, G., Silva, A. O. S., & Meili, L. (2020). Adsorption of anti-inflammatory drug diclofenac by MgAl/layered double hydroxide supported on Syagrus coronata biochar. *Powder Technology, 364*, 229–240. https://doi.org/10.1016/j.powtec.2020.01.083

Empinotti, V. L., Budds, J., & Aversa, M. (2019). Governance and water security: The role of the water institutional framework in the 2013–15 water crisis in São Paulo, Brazil. *Geoforum, 98*, 46–54. https://doi.org/10.1016/j.geoforum.2018.09.022

Enaime, G., Ennaciri, K., Ounas, A., Baçaui, A., Seffen, M., Selmi, T., & Yaacoubi, A. (2017). Preparation and characterization of activated carbons from olive wastes by physical and chemical activation: application to Indigo carmine adsorption. *Journal of Materials and Environmental Science, 8*(11), 4125–4137.

Ezzati, R. (2020). Derivation of pseudo-first-order, pseudo-second-order and modified pseudo-first-order rate equations from Langmuir and Freundlich isotherms for adsorption. *Chemical Engineering Journal, 392*, 123705–123717. https://doi.org/10.1016/j.cej.2019.123705

Figueiredo, V. M., Lourenço, J. B., De Vasconsellos, N. J. S., & Da Silva, W. L. (2020). Preparation, characterization and photocatalytic activity of activated charcoal from microalgae for photocatalytic degradation of Rhodamine B dye. *Cerâmica, 66*, 367–372. https://doi.org/10.1590/0366-69132020663802937

Freundlich, H. (1906). Over the adsorption in solution. *Physical Chemistry, 57*, 384–410. https://doi.org/10.1515/zpch-1907-5723

Gallo-Cordova, A., Silva-Gordillo, M. M., Muñoz, G. A., Arboleda-Faini, X., & Streitwieser, D. A. (2017). Comparison of the adsorption capacity of organic compounds present in produced water with commercially obtained walnut shell and residual biomass. *Journal of Environmental Chemical Engineering, 5*, 4041–4050. https://doi.org/10.1016/j.jece.2017.07.052

Ghenaatgar, A., Tehrani, R. M. A., & Khadir, A. (2019). Photocatalytic degradation and mineralization of dexamethasone using WO_3 and ZrO_2 nanoparticles: Optimization of operational parameters and kinetic studies. *Journal of Water Process Engineering, 32*, 100969–100977. https://doi.org/10.1016/j.jwpe.2019.100969

Halpin, D. M. G., Singh, D., & Hadfield, R. M. (2020). Inhaled corticosteroids and COVID-19: A systematic review and clinical perspective. *European Respiratory Journal, 55*, 2001009–2001017. https://doi.org/10.1183/13993003.01009-2020

Hubbe, M. A., Azizian, S., & Douven, S. (2019). Implications of apparent pseudo-second-order adsorption kinetics onto cellulosic materials: A review. *BioRes., 14*, 7582–7626.

Kebede, T. G., Seroto, M. B., Chokwe, R. C., Dube, S., & Nindi, M. M. (2020). Adsorption of antiretroviral (ARVs) and related drugs from environmental wastewaters using nanofibers. *Journal of Environmental Chemical Engineering, 8*, 104049–104059. https://doi.org/10.1016/j.jece.2020.104049

Keshtkar, M., Dobaradaran, S., Keshmiri, S., Ramavandi, B., Arfaeinia, H., & Ghaedi, H. (2019). Effective parameters, equilibrium, and kinetics of fluoride adsorption on Prosopis cineraria and *Syzygium cumini* leave. *Environmental Progress and Sustainable, 38*, 429–440. https://doi.org/10.1002/ep.13118

Kumar, K. V., Gadipelli, S., Wood, B., Ramisetty, K. A., Stewart, A. A., Howard, C. A., Brett, D. J. L., & Reinoso, F. R. (2019). Characterization of the adsorption site energies and heterogeneous surfaces of porous materials. *Journal of Materials Chemistry A, 7*, 10104–10137. https://doi.org/10.1039/c9ta00287a

Kumar, K. V., Gadipelli, S., Howard, C. A., Kwapinski, W., & Brett, D. J. L. (2021). Probing adsorbent heterogeneity using Toth isotherms. *Journal of Materials Chemistry A, 9*, 944–962. https://doi.org/10.1039/d0ta08150g

Lagergren, S. (1898). About the theory of so-called adsorption of soluble substances. *Kungliga Svenska Vetenskapsakademiens*, *24*, 1–39.

Langmuir, I. (1918). The adsorption of gases on plane surfaces of glass, mica and platinum. *Journal of the American Chemical Society, 40*, 1361–1403. https://doi.org/10.1021/ja02242a004

Liu, G., Qiu, L., Deng, H., Wang, J., Yao, L., & Deng, L. (2020). Ultrahigh surface area carbon nanosheets derived from lotus leaf with super capacities for capacitive deionization and dye adsorption. *Applied Surface Science, 524*, 146485–146495. https://doi.org/10.1016/j.apsusc.2020.146485

Nguyen, V. T., Nguyen, T. M. T., Liu, Y., Cai, Q. (2021). Fabrication of partially graphitic biochar for the removal of diclofenac and ibuprofen from aqueous solution: Laboratory conditions and real sample applications, Environmental Engineering Science. 1–16. https://doi.org/10.1089/ees.2020.0202.

Nunes, L. L. A. & Lima, T. M. (2020). Pharmacotherapy for covid-19 treatment in patients with renal impairment: an updated review, Scielo. https://doi.org/10.1590/SciELOPreprints.384.

Pavlović, S. M., Marinković, D. M., Kostić, M. D., Lončarević, D. R., Mojović, L. V., Stanković, M. V., & Veljković, V. B. (2021). The chicken eggshell calcium oxide ultrasonically dispersed over lignite coal fly ash-based cancrinite zeolite support as a catalyst for biodiesel production. *Fuel, 289*, 119912–119922. https://doi.org/10.1016/j.fuel.2020.119912

Roozbeh, M., Babaie-Kafaki, S., & Aminifard, Z. (2020). Two penalized mixed–integer nonlinear programming approaches to tackle multicollinearity and outliers

effects in linear regression models. *Journal of Industrial and Management Optimization, 17*, 3475–3491. https://doi.org/10.3934/jimo.2020128

Sastry, N. V., Singh, D. K., Thummar, A. D., Verma, G., & Hassan, P. A. (2016). Effect of hydrocarbon surfactants on dexamethasone solubilization into silicone surfactant micelles in aqueous media and its release from agar films as carriers. *Journal of Molecular Liquids, 225*, 11–19. https://doi.org/10.1016/j.molliq.2016.11.034

Sethy, N. K., Arif, Z., Mishra, P. K., & Kumar, P. (2020). Green synthesis of TiO_2 nanoparticles from *Syzygium cumini* extract for photo-catalytic removal of lead (Pb) in explosive industrial wastewater. *Green Processing and Synthesis, 9*, 171–181. https://doi.org/10.1515/gps-2020-0018

Shahri, F. B., Niazi, A., & Akrami, A. (2018). Application of full factorial design for removal of polycyclic aromatic dye from aqueous solution using 4A zeolite: Adsorption isotherms, thermodynamic and kinetic studies. *Polycyclic Aromatic Compounds, 38*, 141–156. https://doi.org/10.1080/10406638.2016.1173074

Sips, R. (1948). On the structure of a catalyst surface. *The Journal of Chemical Physics, 16*, 490–495. https://doi.org/10.1063/1.1746922

Smiljanić, D., De Gennaro, B., Daković, A., Galzerano, B., Germinario, C., Izzo, F., Rottinghaus, G. E., & Langella, A. (2021). Removal of non-steroidal anti-inflammatory drugs from water by zeolite-rich composites: The interference of inorganic anions on the ibuprofen and naproxen adsorption. *Journal of Environmental Management, 286*, 112168–112177. https://doi.org/10.1016/j.jenvman.2021.112168

Srivatsav, P., Bhargav, B. S., Shanmugasundaram, V., Arun, J., Gopinath, K. P., & Bhatnagar, A. (2020). Biochar as an eco-friendly and economical adsorbent for the removal of colorants (dyes) from aqueous environment: A review. *Water, 12*, 3561–3588. https://doi.org/10.3390/w12123561

Sterne, J. A. C. (2020). Association between administration of systemic corticosteroids and mortality among critically ill patients with COVID-19: A meta-analysis. *JAMA, 324*, 1330–1341. https://doi.org/10.1001/jama.2020.17023

Thiebault, T. (2020). Raw and modified clays and clay minerals for the removal of pharmaceutical products from aqueous solutions: State of the art and future perspectives. *Critical Reviews in Environmental Science and Technology, 50*, 1451–1514. https://doi.org/10.1080/10643389.2019.1663065

Tirkey, P., Bhattacharya, T., & Chakraborty, S. (2018). Optimization of fluoride removal from aqueous solution using Jamun (*Syzygium cumini*) leaf ash. *Process Safety and Environmental, 115*, 125–138. https://doi.org/10.1016/j.psep.2017.1

Tóth, J. (1981). A uniform interpretation of gas/solid adsorption. *Journal of Colloid and Interface Science, 79*, 85–95. https://doi.org/10.1016/0021-9797(81)90050-3

Wang, D., Luo, H., Liu, L., Wei, W., & Li, L. (2019). Adsorption characteristics and degradation mechanism of metronidazole on the surface of photocatalyst TiO_2: A theoretical study. *Applied Surface Science, 478*, 896–905. https://doi.org/10.1016/j.apsusc.2019.02.052

Wang, R., Shi, M., Xu, F., Qiu, Y., Zhang, P., Shen, K., Zhao, Q., Yu, J., & Zhang, Y. (2020). Graphdiyne-modified TiO_2 nanofibers with osteoinductive and enhanced photocatalytic antibacterial activities to prevent implant infection. *Nature Communications, 11*, 1–12. https://doi.org/10.1038/s41467-020-18267-1

Weber, W. J., & Morris, J. C. (1963). Kinetics of adsorption on carbon from solutions. *Journal of the Sanitary Engineering Division, 89*, 31–39. https://doi.org/10.1061/JSEDAI.0000430

Yanyan, L., Kurniawan, T. A., Zhu, M., Ouyang, T., Avtar, R., Othman, M. H. D., Mohammad, B. T., & Albadarin, A. B. (2018). Removal of acetaminophen from synthetic wastewater in a fixed-bed column adsorption using low-cost coconut shell waste pretreated with NaOH, HNO_3, ozone, and/or chitosan. *Journal of Environmental Management, 226*, 365–376. https://doi.org/10.1016/j.jenvman.2018.08.032

Zhang, M., Meng, J., Liu, Q., Gu, S., Zhao, L., & Dong, M. (2019b). Corn stover–derived biochar for efficient adsorption of oxytetracycline from wastewater. *Journal of Materials Research, 34*, 3050–3060. https://doi.org/10.1557/jmr.2019.198

Zhang, W., Zhao, Y., Zhang, F., Wang, Q., Li, T., Liu, Z., Wang, J., Qin, Y., Zhang, X., Yan, X., Zeng, X., & Zhang, S. (2020). The use of anti-inflammatory drugs in the treatment of people with severe coronavirus disease 2019 (COVID-19): The experience of clinical immunologists from China. *Clinical Immunology, 214*, 108393–108398. https://doi.org/10.1016/j.clim.2020.108393

Zhu, G., Xu, H., Dufresne, A., & Lin, N. (2018). High-adsorption, self-extinguishing, thermal, and acoustic-resistance aerogels based on organic and inorganic waste valorization from cellulose nanocrystals and red mud. *ACS Sustainable Chemistry & Engineering, 6*, 7168–7180. https://doi.org/10.1021/acssuschemeng.8b01244

Zidi, Z., Ltifi, M., Ayadi, Z. B., Mir, L. E., & Nóvoa, X. R. (2019). Effect of nano-ZnO on mechanical and thermal properties of geopolymer. *Journal of Asian Ceramic Societies, 8*, 1–9. https://doi.org/10.1080/21870764.2019.1693682